Chemical Geology 685 (2025) 122812

Contents lists available at ScienceDirect

Chemical Geology

journal homepage: www.elsevier.com/locate/chemgeo

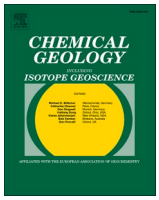

Hydrogen diffusion in apatite normal to the c-axis: Estimation of hydrogen diffusing species

Chikashi Yoshimoto [a,*], Shoichi Itoh [a,*], Isao Sakaguchi [b]

[a] Division of Earth and Planetary Science, Kyoto University, Oiwakecho Sakyo-ku Kyoto-shi, Kyoto 606-8502, Japan
[b] National Institute for Materials Science, 1-1 Namiki, Tsukuba, Ibaraki 305-0044, Japan

ARTICLE INFO

Editor: Claudia Romano

Keywords:
Apatite
Hydrogen diffusion
Hydrogen isotopic composition
H_2O
SIMS

ABSTRACT

Hydrogen isotope retention of apatite is important in discussing hydrogen isotopic compositions in natural apatite. In order to estimate hydrogen isotopic variations associated with thermal processes, experiments on the normal diffusion of fluorapatite along the c-axis using ^2H_2O vapor as a diffusion source were performed at 550–700 °C. The diffusion coefficients of fluorapatite were determined by secondary ion mass spectrometry (SIMS). Depth profiles of diffusion were obtained by SIMS, and diffusion coefficients were obtained by model fitting. The Arrhenius relationship for fluorapatite normal to the c-axis yielded a pre-exponential factor (D_0) = 9.77×10^{-6} [m^2/s] and activation energy (E_a) = 208 ± 27 [kJ/mol] over the temperature range of the experiment. The diffusion coefficient normal to the c-axis was approximately three times greater than that parallel to the c-axis and the activation energies from both crystal orientations were consistent within the error margin. The difference in diffusion coefficients can be explained by using the nearest oxygen site and considering the diffusion mechanism with OH^- as the diffusing species. Based on the similarity of the diffusion mechanism with crystallographic orientation, a closure temperature was calculated using the results of this study. This updated closure temperature is useful for discussing the retention of hydrogen isotopes and for determining the cooling rate from the hydrogen isotopic compositions in natural water-rock interaction under asteroids, planets, and terrestrial geological setting.

1. Introduction

Hydrogen is the most abundant element in the solar system. How hydrogen has migrated from space to the Earth's deep interior over the time scale from the primitive solar system to the present is of great interest. Hydrogen isotopic composition in minerals is an important tracer for the origin and evolution of water in solar-system bodies, including the Earth (e.g. Graham et al., 1984). In order to use hydrogen isotope signatures in hydrous minerals to ascertain source characteristics, an understanding of how theses signatures can be altered due to hydrous alteration needs to be understood. Therefore, it is necessary to understand the hydrogen diffusivity in apatite during water-rock interactions. There are several diffusion studies of hydrogen diffusion in hydrous minerals(e.g., zoisite; Graham, 1981, ilvaite; Yaqian and Jibao, 1993, actinolite; Graham et al., 1984 from Suzuoki and Epstein, 1976, tremolite, hornblende; Graham et al., 1984). Obtaining the diffusion coefficient of hydrogen not only quantifies its isotopic retention, but also its temperature dependence, which allows us to estimate the diffusing species. Estimation of the diffusing species provides information on the magnitude of the isotope effect when considering hydrogen isotopic variations. The activation energy estimated from the temperature dependence of hydrogen diffusion in hydrous minerals is around 100 kJ/mol, which indicates that the diffusing species of hydrogen in these minerals are protons.

Apatite, a hydrous mineral, has been particularly studied due to its occurrence in a wide range of solar-system bodies, such as the Earth (e.g., Piccoli and Candela, 1994), the Moon (e.g., McCubbin et al., 2010), Martian meteorites (e.g., Greenwood et al., 2008; McCubbin and Nekvasil, 2008), chondrites (e.g., Ebihara and Honda, 1987; Göpel et al., 1994), achondrites (e.g., Steele and Smith, 1982), and Ryugu (e.g., (Yokoyama et al., 2022). Apatite is a mineral that can be dated in various ways and is more resistant to metamorphism and alteration than other hydrous minerals, making it possible to discuss the origin and evolution of water in relation to its chronology. Apatite is a type of phosphate mineral with the chemical formula $Ca_5(PO_4)_3(F,Cl,OH)$, and has three endmember components: hydroxyapatite ($Ca_5(PO_4)_3OH$), fluorapatite

* Corresponding authors.
E-mail addresses: yoshimoto.chikashi.c68@kyoto-u.jp (C. Yoshimoto), sitoh@kueps.kyoto-u.ac.jp (S. Itoh).

https://doi.org/10.1016/j.chemgeo.2025.122812
Received 1 November 2024; Received in revised form 11 April 2025; Accepted 24 April 2025
Available online 26 April 2025

($Ca_5(PO_4)_3F$), and chlorapatite ($Ca_5(PO_4)_3Cl$). Hydrogen is contained not only in hydroxyapatite but also in fluorapatite and chlorapatite. For these reasons, apatite is a useful mineral for hydrogen isotopic composition measurements.

Recently, Yoshimoto et al. (2024) reported hydrogen diffusion in apatite using a $^2H_2O/O_2$ vapor flow system. The total concentration of hydrogen and deuterium obtained from secondary ion mass spectrometry measurements was constant, indicating hydrogen self-diffusion; the hydrogen diffusion coefficient results for the apatite c-axis parallel at 550–700 °C indicate that hydrogen self-diffusion can sufficiently change the hydrogen isotopic composition, not only F-Cl-OH interdiffusion as reported by Brenan (1993) and Li et al. (2020). The activation energy for hydrogen diffusion at 550–700 °C reported by Yoshimoto et al. (2024) was 205 kJ/mol. Since this is consistent with the activation energy of oxygen diffusion Farver and Giletti (1989), it was proposed that a diffusion mechanism is using oxygen sites and OH^- is as the diffusing species. However, since apatite has a hexagonal crystal structure, the hydrogen isotopic composition of natural apatite cannot be estimated unless the diffusion coefficient is determined not only parallel to the c-axis but also normal to the c-axis and the diffusion mechanism is identified. In fact, differences in diffusion coefficients have been observed in the diffusion of other elements in apatite (e.g., Farver and Giletti, 1989). Therefore, in this study, in order to estimate hydrogen isotopic variations in natural apatite, we present hydrogen diffusion coefficients normal to the c-axis and propose a hydrogen diffusion mechanism. In addition, to discuss the hydrogen isotope retention of natural apatite, the relationship between closure temperature and cooling rate was calculated from the obtained diffusion coefficients.

2. Experimental methods

2.1. Sample selection and preparation

Natural fluorapatite from Durango, Mexico, was used in this study. Durango apatite is readily available in large sizes and *gem* quality, its mineralogy is well studied (e.g., Young et al., 1969; Hughes et al., 1989), it is used in studies of the physicochemical properties of apatite, including diffusion experiments (e.g., Farver and Giletti, 1989; Brenan, 1993; Cherniak, 2005; Higashi et al., 2017; Yoshimoto et al., 2024). Among the rare earth elements, La, Ce, and Nd were each present at concentrations of several thousand ppm (Higashi et al., 2017). The water content of Durango apatite is reported to be 500–1000 ppm H_2O (e.g., McCubbin et al., 2015; Greenwood, 2018).

One Durango fluorapatite single crystal was used for the experiments. The apatite sample was cut into slabs approximately 2 mm thick both parallel to the c-axis and the a-axis for diffusion experiments normal to the c-axis, using a low-speed diamond saw. Multiple sections were obtained from a single apatite crystal. The cut surfaces of the specimens were polished to a specular surface using several grades of diamond paste and vibratory polishing by chemical polishing. The chemical polishing was to remove microscopic dislocations and other defects caused by polishing (see Yurimoto et al., 1989; Sakaguchi et al., 1992; Yoshimoto et al., 2024). The polished samples were then ultrasonically cleaned with ethanol, detergent water, deionized water, and deionized hot water.

2.2. Pre-annealing treatment

Pre-annealing is effective in removing defects, dislocations, and other damage in the crystal. In previous studies, pre-annealing of apatite has been performed at temperatures above 1000 °C (e.g., Cherniak, 2005); Yoshimoto et al. (2024) avoided loss of volatiles from the apatite surface in the process, and the pre-annealing process is not performed. The hydrogen-deuterium diffusion profiles in Fig. 3 of Higashi et al. (2017) show a discrepancy between the depth profiling data and the fitting curves in the deeper regions. Such discrepant diffusion profiles are referred to as "tailing" profiles. Tailing diffusion profiles are thought to be caused by the presence of ionic pathways outside the crystal lattice such as defects and dislocations (Zhang et al., 2007). Yoshimoto et al. (2024) attempted to remove it by chemical polishing and succeeded in obtaining tailing-free diffusion. Chemical polishing did not result in a well-resolved diffusion profile normal to the c-axis, likely due to anisotropy associated with crystal orientation.

Fig. S2 in supplementary materials shows a typical diffusion profile of apatite crystals annealed at 600 °C for 14,400 s under $^2H_2O/O_2$ conditions without pre-annealing and its fitting curve by error function. In Fig. S2, the fitting curve is in good agreement with the diffusion profile in the region from the sample surface to a depth of 300 nm. On the other hand, in the region deeper than 300 nm, there is a large discrepancy between the diffusion profile and the fitting curve. This region is the tailing region, and diffusion through this region could be faster than volume diffusion. In order to evaluate the effect of fast diffusion on the profile down to this 300 nm depth, a comparison with a profile in which tailing is almost eliminated by the pre-annealing treatment is necessary. See Supplementary Materials for details on the removal of fast diffusion by pre-annealing and its effect on diffusion coefficients.

Pre-annealing was performed on the diffusion samples (Ap_12b, Ap_14b) at 650 °C and 600 °C. These samples were prepared by regrinding Ap_12a and Ap_14a, respectively, which had been previously used in diffusion experiments. The affected surface layers from the initial experiments were completely removed by polishing before re-experiment. It was performed at 700 °C for about 3 h in a mixed H_2O/O_2 gas atmosphere using a Kyoto University reactor (Heat Tec, Kanagawa, Japan). The pure water reservoir was maintained at 85 °C, the oxygen carrier gas passed through the H_2O, and the sample was exposed to the H_2O/O_2 mixture (~0.57 atm H_2O, saturation vapor pressure at 85 °C, as calculated by Tetens, 1930). The flow rate of the oxygen carrier gas was 600 sccm (standard cubic centimeters per minute) at 1 atm. To take care of ^1H contamination in subsequent diffusion annealing experiments, the reactors were co-washed with a mixture of ^2H_2O and O_2 gas at approximately 300 °C for about 1 h after the pre-annealing treatment.

2.3. Diffusion annealing experiments

Hydrogen diffusion experiments using apatite slices were performed in a reactor at Kyoto University (Yoshimoto et al., 2024). The experimental technique is the same as that of Yoshimoto et al. (2024). The temperature of the hydrogen diffusion treatment ranged from 550 °C to 700 °C. The annealing duration ranged from 3600 s (at 700 °C) to 57,600 s (at 550 °C). To eliminate adsorbed water on the sample surfaces, apatite slices were heated at 150 °C for 3600 s under dry flow before each diffusion annealing experiment.

2.4. SIMS analysis

SIMS (Cameca 4f-E7, Kyoto University) was used to obtain ^2H concentration vs. depth profiles of the apatite samples.After experiments, apatite was coated with Au (~50 nm) and held in the airlock for >1 day to remove surface adsorbed water contamination. A 14.5 kV accelerated $^{133}Cs^+$ primary ion beam, current 3–5 nA, spot size ~15 μm was used for all measurements. The primary ion beam was rasterized to 150 μm × 150 μm at each analysis point, forming a flat crater on the surface of the apatite sample. To avoid contamination by residual hydrogen in the sample chamber, the vacuum was maintained below 5×10^{-8} Pa during the measurement (using a large liquid nitrogen cold trap system manufactured by Techno IS Co.) Sputtered secondary ions were acquired from a central region ~30 μm in diameter that was cut out using a mechanical aperture to minimize artifacts arising from the crater edge of the primary ion beam. A normal-incident electron gun (acceleration voltage 4.5 kV) was used for charge compensation. Negative secondary

ions $^{1}H^{-}$, $^{2}H^{-}$, and $^{18}O^{-}$ were sequentially acquired using an electron multiplier for 1 s per cycle. Each crater depth from SIMS was measured using a surface profiler (Surfcorder ET200; Kosaka Laboratory, Osaka, Japan) and measurement times were converted to depths.

2.5. Calculation of diffusion coefficients

To get the diffusion coefficient (D), the profile of $C[^{2}H] = {}^{2}H/({}^{1}H + {}^{2}H)$ was adjusted to fit the solution of the diffusion equation obtained by assuming $C[^{2}H]$ at the surface and diffusion in a semi-infinite medium (Crank, 1975). The diffusion profiles were fitted to the following least-squares equation:

$$\left(\frac{C_{(x,t)} - C_0}{C_s - C_0}\right) = \mathrm{erfc}\left(\frac{x}{2\sqrt{Dt}}\right). \quad (1)$$

Where $C_{(x,\ t)}$ is isotopic concentration at depth x from the surface, also denoted as $C[^{2}H]$; $C_s = C_{(0,\ t)}$ is surface concentration; $C_0 = C_{(x,\ 0)}$ is background concentration; D is diffusion coefficient; t is duration of diffusion experiment; and erfc is the complementary error function.

3. Results

3.1. Hydrogen diffusion profiles

The isotopic concentration of ^{2}H, expressed as $C[^{2}H]$ (calculated as $^{2}H/(^{1}H + {}^{2}H)$) in the experiment at 650 °C is shown in Fig. 1. The $C[^{2}H]$ at the surface is about 0.6 and decreases linearly with depth on the log scale. The blue fitting curve fitted using Eq. (1) fits well with the depth data from the surface to background, yielding a D of 1.82×10^{-17} m^2/s. The values of diffusion coefficients for each temperature obtained by fitting diffusion data at other temperatures and their mean values and standard deviations are shown in Table 1. The diffusion coefficient of hydrogen in apatite was $5.98 \pm 0.47 \times 10^{-19}$ m^2/s at 550 °C and $5.78 \pm 0.14 \times 10^{-17}$ m^2/s at 700 °C.

3.2. Temperature dependence of hydrogen diffusion in apatite

D generally exhibits temperature dependence, as expressed by the Arrhenius equation:

$$D = D_0 \exp\left(-\frac{E_a}{RT}\right), \quad (2)$$

where D_0 is a pre-exponential (frequency) factor, E_a the activation energy, and T the temperature. Fig. 2 illustrates the Arrhenius relationship for hydrogen diffusion in Durango apatite parallel to the c-axis at

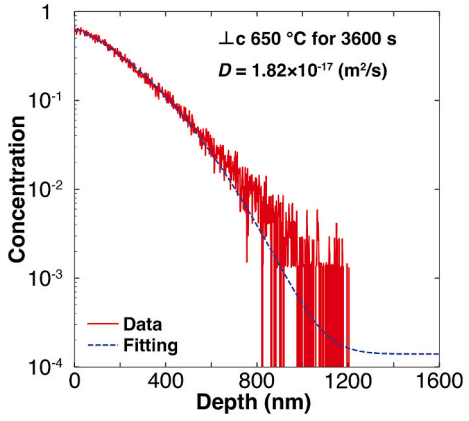

Fig. 1. Representative diffusion profile of the concentration ($C[^{2}H] = {}^{2}H/({}^{1}H + {}^{2}H)$) with depth in apatite crystal, which was tested in hydrothermal condition for 3600 s at 650 °C; least-squares linear regression was performed fit to the data points.

Table 1
Hydrogen diffusion coefficients in apatite and ratio to parallel to the c-axis.

Sample	T (°C)	Time (s)	D (m^2/s)
Ap_13a	550	57,600	6.32×10^{-19}
	550	57,600	5.68×10^{-19}
	550	57,600	6.54×10^{-19}
	550	57,600	5.48×10^{-19}
		mean (σ)	$5.98 \pm 0.47 \times 10^{-19}$
		ratio to //c (σ)	2.84 ± 0.48
Ap_12a*	600	14,400	2.62×10^{-18}
	600	14,400	3.03×10^{-18}
	600	14,400	2.78×10^{-18}
Ap_12b*	600	14,400	4.84×10^{-18}
	600	14,400	1.76×10^{-18}
	600	14,400	3.52×10^{-18}
		mean (σ)	$2.97 \pm 1.07 \times 10^{-18}$
		ratio to //c (σ)	3.09 ± 0.41
Ap_14b*	650	3600	1.55×10^{-17}
	650	3600	1.58×10^{-17}
	650	3600	1.77×10^{-17}
	650	3600	1.56×10^{-17}
		mean (σ)	$1.62 \pm 0.10 \times 10^{-17}$
		ratio to //c (σ)	3.10 ± 0.38
Ap_14a*	700	3600	5.76×10^{-17}
	700	3600	5.66×10^{-17}
	700	3600	5.93×10^{-17}
		mean (σ)	$5.78 \pm 0.14 \times 10^{-17}$
		ratio to //c (σ)	3.18 ± 0.74

The errors (σ) are the standard deviation for each analysis.
* it means same slice and Ap12b and Ap14b are pre-annealed after polishing Ap12a and Ap14a respectively.

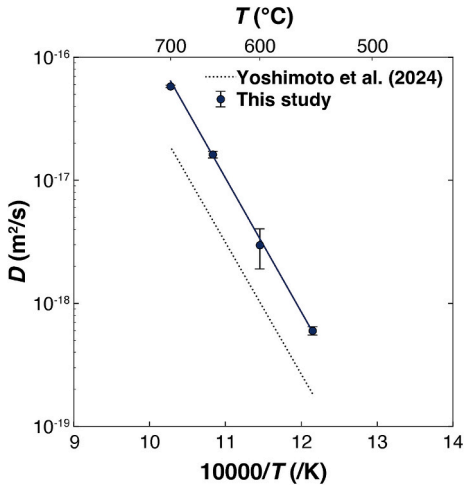

Fig. 2. Arrhenius plots of hydrogen self-diffusion results for apatite, showing diffusion coefficient results at each temperature and their least-squares fitting in two studies (this study and Yoshimoto et al., 2024).

550 °C–700 °C, which is expressed as

$$D = 9.77 \times 10^{-6} \exp\left(-\frac{208 \pm 27\mathrm{kJ/mol}]}{RT}\right) [\mathrm{m^2/s}]$$

Fig. 2 shows an Arrhenius plot of the diffusion coefficient as a function of temperature. Fig. 2 also shows the temperature dependence of the diffusion coefficients for Durango apatite parallel to the c-axis. The diffusion coefficients normal to the c-axis are approximately 3 times faster than that parallel to the c-axis for each temperature. However, the activation energy of 208 ± 27 [kJ/mol] for normal to the c-axis hydrogen diffusion in the present study agrees with the activation energy of 205 ± 11 [kJ/mol] obtained from the experiment for parallel to the c-axis direction within the margin of error.

4. Discussion

4.1. Diffusion mechanism of hydrogen in apatite

The activation energies obtained from the temperature dependence are consistent within a margin of error with those obtained from experiments parallel to the c-axis, indicating that the diffusion mechanisms are similar. Yoshimoto et al. (2024) proposed a diffusion mechanism using OH^- as the diffusing species with oxygen sites based on the similarity with the activation energy of oxygen diffusion (Farver and Giletti, 1989). The activation energy of about 200 kJ/mol is large for the Grotthuss mechanism. Considering the similarity of the activation energy with oxygen diffusion, it is reasonable to consider OH^- as a diffusing species for hydrogen diffusion through oxygen vacancies. For OH^- diffusion through vacancies, the diffusion coefficient is given by the following Eq. (3):

$$D = D_0 \exp\left(-\frac{H_f^{V_o} + H_m^{OH}}{RT}\right), \tag{3}$$

Where $H_f^{V_o}$ is the enthalpy of formation of oxygen vacancy, H_m^{OH} is transfer enthalpy involved in the jumps of OH^- into oxygen vacancies. Comparing Eq. (2) and Eq. (3), it can be seen that the activation energy of diffusion is the sum of $H_f^{V_o}$ and H_m^{OH}. Considering the simple bond valence theory, oxygen ions with large valence diffuse more slowly and have larger activation energies than OH^- ions. However, when $H_f^{V_o} > H_m^{OH}$, the activation energy of diffusion is mainly provided by $H_f^{V_o}$, consistent with the similarity of the activation energy with oxygen diffusion. Furthermore, the activation energy of OH^- calculated by this study and Yoshimoto et al. (2024), about 200 kJ/mol, is significantly lower than that of OH^- self-diffusion, about 400 kJ/mol, in Li et al. (2020). As discussed in Yoshimoto et al. (2024), the discrepancy in activation energy between them is likely due to fundamental differences in diffusion mechanisms. While Li et al. (2020) derived OH^- self-diffusion coefficients from F-Cl-OH inter-diffusion profiles, which may reflect site-specific exchange processes. Yoshimoto et al. (2024) obtained hydrogen diffusivity directly under hydrothermal conditions using ^2H_2O vapor in fluorapatite, where diffusion is more likely controlled by migration through oxygen sites rather than isolated OH^- site hopping.

As shown in Table 1, the diffusion coefficients at each temperature are 2.8–3.2 times larger than those for the parallel to the c-axis. Although pre-annealing at 600 °C effectively reduced the tail in the diffusion profile, it did not significantly affect the calculated diffusion coefficient. This indicates that the apparent profile tail is likely due to near-surface damages or natural dislocation, rather than changes in the bulk diffusion behavior. If OH^- diffusion is mainly controlled by the concentration of oxygen vacancies, the lack of change in diffusivity despite pre-annealing suggests that pre-annealing did not substantially affect the oxygen vacancy concentration. It is more reasonable to infer that pre-annealing primarily reduced the density of fast diffusion pathways. In this section, we discuss the diffusion mechanism focusing on the difference in the magnitude of the diffusion coefficients.

Fluorapatite has a hexagonal crystal structure with space group $P6_3/m$ (Hughes et al., 1989; Hughes and Rakovan, 2015). Fig. 3 shows the crystal structure of apatite drawn using VESTA(Momma and Izumi, 2008); we used the crystal data for Durango apatite from Hughes et al. (1989). The apatite structure has three cation sites, M1, M2, and T. The M1 site is $Ca(1)O_9$, the M2 site is $Ca(2)O_5XO$ polyhedral with X = F, Cl, and OH, and the T site is PO_4 tetrahedral. In the apatite structure, hydrogen atoms are stable at the X-site as OH. To consider the migration pathway with OH^- as the diffusing species, the migration from one X-site to another is considered as a jump between the OH and oxygen sites in the unit lattice. In the drawn crystal structure, there are six possible jumps from an X-site to an oxygen site, and after that, the choices of

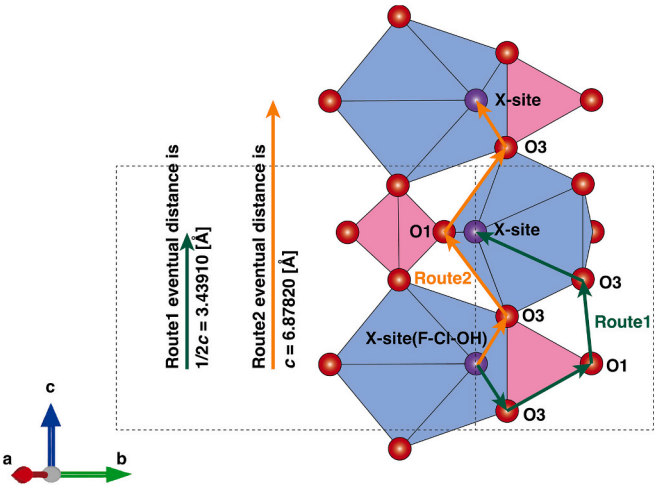

Fig. 3. Schematic diagram of hydrogen diffusion mechanism parallel to the c-axis. Two routes (route 1 and route 2) are possible for the migration from one X site to another X site using nearby oxygen sites. The final migration distances for each route are 3.43910 and 6.87820 [Å].

possible jumps increase even more. Here we describe the migration path of the diffuse species to the other X-sites with jumps to the nearest sites to avoid complexity and with fewer jumps. The distance between neighboring sites in apatite crystals was determined using VESTA. If each jump distance is short and easy to jump, two patterns are expected for the movement between X-sites in the c-axis direction and one pattern in the a-axis direction. Table 2 shows the travel paths and jump distances for each. Fig. 3 shows Route 1 and Route 2 for the c-axis direction. Route 1 moves to an X-site $1/2c$ away, whereas Route 2 moves to an X-site c away. Fig. 4 shows route 3, which moves a in the direction of the a-axis. The number of jumps is the same for all routes. Since the activation energies for hydrogen diffusion parallel and normal to the c-axis are indistinguishable within error, it is reasonable to infer that the rate-limiting step is shared between the two crystallographic directions. Specifically, the jump between the X-site and the O3 oxygen site (X ↔ O3), which is common to both diffusion pathways, is likely to represent the rate-limiting process. The ratios of the diffusion coefficients in each direction of the experiments and the distance moved between the X-sites are compared: since the axial lengths of the Durango apatite are c = 6.87820 [Å] and a = 9.39730 [Å], the length ratios of the possible routes are expressed as follows:

$$\frac{\sqrt{3}}{2}a \Big/ \frac{1}{2}c = 2.366 \ (\text{neighboring, Route1/Route3}), \tag{4}$$

$$\frac{\sqrt{3}}{2}a \Big/ c = 1.183 \ (\text{skipping over, Route2/Route3}) \tag{5}$$

The $\sqrt{3}/2$ factor is used to compensate for the experimentally determined direction normal to both the a-axis and the c-axis. Since the diffusion length x is expressed as $x = \sqrt{Dt}$ (t is diffusing time), the square root of the ratio of the experimental value and the length ratio are compared. The square root of diffusion coefficients between normal and parallel to the c-axis is ranged in 1.69–1.78 (Table 1) and is in the ratios of the eventual distance (Eqs. (3) and (4)). The above results suggest that OH^- jumps between oxygen sites as a diffusing species regardless of crystallographic direction, and that the difference in diffusion coefficients depending on crystallographic direction is due to the difference in the eventual distance of OH^- migration in the lattice.

4.2. The comparison between apatite and other hydrous minerals

Hydrogen diffusion in other hydrous minerals than apatite also plays

Table 2
X-site to X-site migration routes.

Route	direction	first step distance (Å)	second step distance (Å)	third step distance (Å)	final step distance (Å)	Eventual distance (Å)
Route1	parallel to the c-axis	3.15 (X-O3)	2.53 (O3-O1)	2.97 (O1-O3)	3.15 (O3-X)	1/2 c = 3.44
Route2	parallel to the c-axis	3.15 (X-O3)	2.97 (O3-O1)	2.97 (O1-O3)	3.15 (O3-X)	c = 6.88
Route3	parallel to the a-axis	3.15 (X-O3)	2.48 (O3-O2)	2.95 (O2-O3)	3.15 (O3-X)	a = 9.40

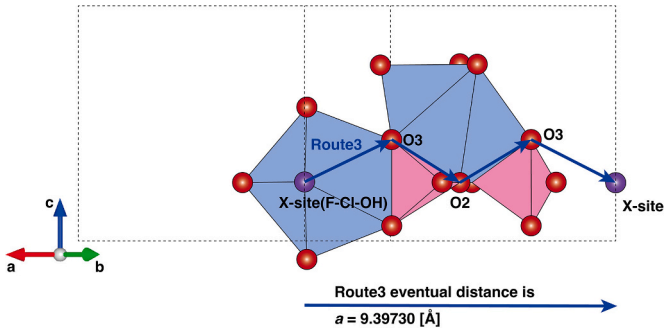

Fig. 4. Schematic diagram of hydrogen diffusion mechanism normal to the c-axis. In the a-axis migration from one X site to another X site using the proximate oxygen sites, only route 3 is considered. The final migration distance is 9.39730 [Å], but a $\sqrt{3}/2$ term must be applied to these distances to correct for the experimental direction.

a very important role. Obtaining diffusion coefficients between different minerals helps to obtain cooling histories in the rock fragments or bodies containing those minerals (e.g., oxygen diffusion; Farver, 1989). Measuring hydrogen isotopic compositions for minerals with different diffusion coefficients and activation energies can constrain closure temperatures and cooling rates for water-related events at relatively low temperatures relative to other elements. From the perspective of studying hydrogen diffusion, on the other hand, it is possible to compare and estimate the diffusion mechanisms. A comparison of the diffusion coefficients obtained in this study with those of other hydrous minerals is shown in Fig. 5. Comparing the diffusion coefficients of these hydrous minerals (zoisite; Graham, 1981, ilvaite; Yaqian and Jibao, 1993, actinolite; Graham et al., 1984 from Suzuoki and Epstein, 1976, tremolite, hornblende; Graham et al., 1984) with those of apatite, there is a significant difference in activation energy for hydrogen diffusion. The

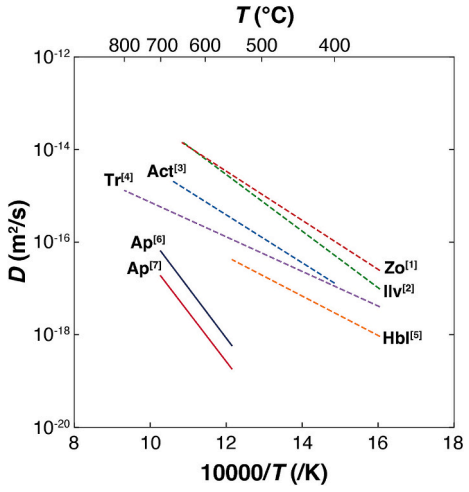

Fig. 5. Several hydrogen diffusion coefficients in hydrous minerals. [1]Zoisite; Graham (1981), [2]Ilvaite; Yaqian and Jibao (1993), [3]Actinolite; Graham et al. (1984) from Suzuoki and Epstein (1976), [4]Tremolite, [5]Hornblende; Graham et al. (1984), [6]Apatite (normal to the c-axis); this study, [7]Apatite (parallel to the c-axis); Yoshimoto et al. (2024).

activation energy of apatite in this study is about 200 kJ/mol, whereas the other hydrous minerals have activation energies in the range of 60–120 kJ/mol.

There are two possible explanations for these differences: first, the diffusion mechanisms of these hydrous minerals, which are silicates, and apatite, which is a phosphate, are different. As mentioned above, the OH^- in the phosphate apatite is suggested to be the diffusing species. Comparison between fluorapatite and hydrous silicates, at low water contents, as in fluorapatite, hydrogen diffusion may occur predominantly via localized hopping of hydroxyl groups. With increasing water content, as in other silicate minerals, the formation of continuous hydrogen-bonding networks could promote long-range proton transfer, potentially involving the Grotthuss mechanism. On the other hand, the low activation energy of other hydrous minerals is said to support the idea that the diffusing species are protons (Norby and Larring, 1997). In considering hydrogen diffusion in solid acids, it is commonly assumed that hydrogen mobility is enhanced in structures containing more acidic anionic groups. Specifically, the PO_4^{3-} is considered more acidic than the SiO_4^{4-}, and thus, hydrogen is expected to diffuse more rapidly and easily in PO_4^{3-} based materials such as apatite. However, this assumption is inconsistent with experimental results: hydrous silicates exhibit higher hydrogen diffusion coefficients and lower activation energies compared to fluorapatite.

The other possibility is that the diffusion coefficient and activation energy may have changed due to polishing, as shown in Yoshimoto et al. (2024). The hydrogen diffusion coefficients of the hydrous minerals shown in the figure were determined by powder experiments and their bulk mass spectrometry. This method does not provide an actual diffusion profile. As Yurimoto et al. (1989) have shown, results of diffusion experiments often show effective diffusion, a mixture of lattice diffusion and fast diffusion due to polishing damages, and in the case of hydrogen, which is considered to diffuse relatively fast, the diffusion profile should be checked more carefully. To verify these results, it will be required to estimate the diffusing species by hydrogen diffusion experiments in sectioned hydrous minerals and their SIMS diffusion profiling and/or molecular dynamics (MD) or Nudged Elastic Band (NEB) simulations.

4.3. Time-temperature conditions for hydrogen in apatite

As an example of the application of diffusion coefficients to natural samples, the retention conditions of the initial hydrogen isotopic composition of apatite will be discussed. An important concept for isotope retention in minerals using diffusion rates is the closure temperature, where the diffusion rate of an element slows sufficiently in a mineral during cooling that isotope exchange practically ceases to occur. By obtaining a relationship between closure temperature and cooling rate, it is also possible to discuss the cooling rate experienced by the sample from isotopic observations of the mineral (Farver, 1989). The relationship between cooling rate (r_0) and closure temperature (T_c) is expressed as follows (Dodson, 1973):

$$T_c = (E_a/R)/\ln\{ARD_0T_c^2/E_al^2r_0\} \quad (6)$$

where E_a = the activation energy for diffusion of the element; R = the universal gas constant; A = a geometric factor dependent on the anisotropy of diffusion; D_0 = the pre-exponential factor for diffusion; l = the effective diffusion radius or halfthickness; r_0 = the initial cooling rate; and T_c = the closure temperature. In this equation, both sides

include T_c, which was conventionally plotted by iterative calculations. However, this equation can be solved about r_0. In this equation, the assumption that reciprocal temperature decreases linearly with time is used; $dT^{-1}/dt = -1/T^2 \bullet dT/dt = const.$. Here, we use this equation for spherical setting. It gives $A = 55.0$ $(12/\pi^2 \bullet (\pi^2/6 \bullet \ln\pi + \sum_1^\infty \ln n/n^2))$ to the geometric factor, and radius to the effective length, l.

The diffusion mechanism of hydrogen in apatite is a similar jump with oxygen vacancies for parallel and normal to the c-axis, and the diffusion coefficients are of the same order. The spherical model can be used for hydrogen diffusion in hexagonal apatite due to faster diffusion normal to the c-axis, without considering extremely fast local diffusion orientations. Fig. 6 shows the results of the above model calculations for different apatite grains of radius 10, 50, and 100 μm, using the hydrogen diffusion coefficient normal to the c-axis determined in this study. Note that outside the experimental temperature range of 550–700 °C, the curves are extrapolations. If it is above this curve for a given temperature and a given initial cooling rate, it indicates that re-equilibration of the hydrogen isotopic composition has occurred. These curves would be very useful when discussing the origin of water using the hydrogen isotopic composition in apatite.

Fig. 6 also shows the closure temperature calculated based on the results of (Higashi et al., 2017), a previous study of hydrogen diffusion in apatite. The hydrogen diffusion coefficients in their study were obtained parallel to the c-axis, where surface damage was not considered, as shown in (Yoshimoto et al., 2024). The hydrogen isotope retention of natural apatite has been discussed using this hydrogen diffusion coefficient. However, it shows that at similar cooling rates of, for example, <10 °C/yr, there is a difference in closure temperature of more than 100 °C. Since the diffusion coefficients of (Higashi et al., 2017) include a diffusion component due to polishing damage, the results of this study should be referred to when discussing the isotopic composition of natural apatite samples more rigorously. Moreover, the diffusing species of hydrogen in oxides has been estimated from the activation energy (~100 kJ/mol) in diffusion experiments, but originally, it was expected that the OH^- would be the diffusing species for hydrogen in oxides.(e.g., Norby and Larring, 1997), which is consisted with the results of this study. Therefore, we would like to strongly suggest that this means that we cannot estimate the transport phenomena of hydrogen in the true geological environment without reconsidering the hydrogen diffusion in other hydrous minerals.

5. Conclusions

The hydrogen diffusion coefficient in fluorapatite perpendicular to the c-axis was determined experimentally using deuterium as a tracer and by depth analysis using SIMS The diffusion coefficient in apatite perpendicular to the c-axis at 550 °C to 700 °C showed the following temperature dependence:

$$D = 9.77 \times 10^{-6} \exp\left(-\frac{208 \pm 27 \mathrm{kJ/mol}]}{RT}\right) [\mathrm{m^2/s}].$$

The diffusion coefficient normal to the c-axis was approximately three times larger than that parallel to the c-axis, and the activation energies matched within error. This suggests that the diffusion mechanism with OH^- as the diffusing species, as discussed by Yoshimoto et al. (2024), is also occurring in the perpendicular c-axis direction. Considering this mechanism, the difference in diffusion coefficients can be explained by the difference in the distance OH^- moves in different crystal orientations. Since the closure temperature calculated using the diffusion coefficient data of this study is more than 100 °C higher than that of Higashi et al. (2017) for slow cooling (<10 °C/yr), the results of this study should be referred to in a more rigorous discussion of hydrogen isotope retention in apatite.

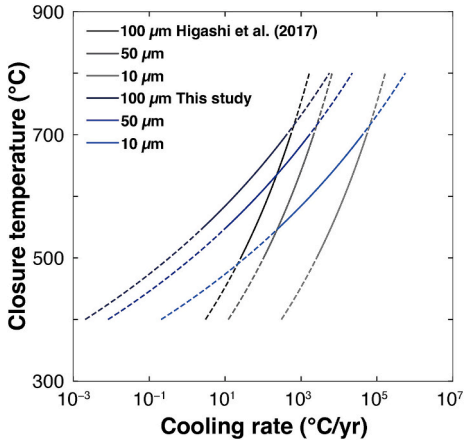

Fig. 6. Closure temperatures calculated based on the diffusion coefficients of this study ($D_{\text{this study}}$) and Higashi et al. (2017) ($D_{\text{polishing damage}}$).

CRediT authorship contribution statement

Chikashi Yoshimoto: Writing – original draft, Visualization, Methodology, Funding acquisition, Formal analysis, Data curation, Conceptualization. **Shoichi Itoh:** Writing – review & editing, Validation, Supervision, Project administration, Methodology, Funding acquisition, Data curation, Conceptualization. **Isao Sakaguchi:** Writing – review & editing, Validation, Supervision, Methodology, Data curation, Conceptualization.

Declaration of competing interest

The authors declare that they have no known competing financial interests or personal relationships that could have appeared to influence the work reported in this paper.

Acknowledgements

We are grateful to Dr. S. Iimura for his help in discussing the hydrogen diffusion mechanisms. This research was partly supported by JSPS KAKENHI (22K18280, 21H04519, 21H04511, 21H01177, 20H01994, 19H00716, 18H04367, 18H01296, 16H01118) and by JST SPRING, Grant Number JPMJSP2110

Appendix A. Supplementary data

Supplementary data to this article can be found online at https://doi.org/10.1016/j.chemgeo.2025.122812.

Data availability

Data will be made available on request.

References

Brenan, J., 1993. Kinetics of fluorine, chlorine and hydroxyl exchange in fluorapatite. Chem. Geol. 110, 195–210. https://doi.org/10.1016/0009-2541(93)90254-G.
Cherniak, D.J., 2005. Uranium and manganese diffusion in apatite. Chem. Geol. 219, 297–308. https://doi.org/10.1016/j.chemgeo.2005.02.014.
Crank, J., 1975. The Mathematics of Diffusion, 2d ed. Clarendon Press, Oxford.
Dodson, M.H., 1973. Closure temperature in cooling geochronological and petrological systems. Contrib. Mineral. Petrol. 40, 259–274. https://doi.org/10.1007/BF00373790.
Ebihara, M., Honda, M., 1987. Rare earth elements in Ca-phosphates of allende carbonaceous chondrite. Meteoritics 22, 179–190. https://doi.org/10.1111/j.1945-5100.1987.tb00618.x.
Farver, J.R., 1989. Oxygen self-diffusion in diopside with application to cooling rate determinations. Earth Planet. Sci. Lett. 92, 386–396. https://doi.org/10.1016/0012-821X(89)90062-9.

Farver, J.R., Giletti, B.J., 1989. Oxygen and strontium diffusion kinetics in apatite and potential applications to thermal history determinations. Geochim. Cosmochim. Acta 53, 1621–1631. https://doi.org/10.1016/0016-7037(89)90243-3.

Göpel, C., Manhès, G., Allègre, C.J., 1994. U-Pb systematics of phosphates from equilibrated ordinary chondrites. Earth Planet. Sci. Lett. 121, 153–171. https://doi.org/10.1016/0012-821X(94)90038-8.

Graham, C.M., 1981. Experimental hydrogen isotope studies III: Diffusion of hydrogen in hydrous minerals, and stable isotope exchange in metamorphic rocks. Contrib. Mineral. Petrol. 76, 216–228. https://doi.org/10.1007/BF00371961.

Graham, C.M., Harmon, R.S., Sheppard, S.M., 1984. Experimental hydrogen isotope studies: hydrogen isotope exchange between amphibole and water. Am. Mineral. 69, 128–138.

Greenwood, J.P., 2018. Hydrogen and D/H analysis of apatite by elemental analyzer-chromium/high-temperature conversion-isotope ratio mass spectrometry (EA-Cr/HTC-IRMS). Chem. Geol. 500, 175–181. https://doi.org/10.1016/j.chemgeo.2018.09.029.

Greenwood, J.P., Itoh, S., Sakamoto, N., Vicenzi, E.P., Yurimoto, H., 2008. Hydrogen isotope evidence for loss of water from Mars through time. Geophys. Res. Lett. 35. https://doi.org/10.1029/2007GL032721.

Higashi, Y., Itoh, S., Hashiguchi, M., Sakata, S., Hirata, T., Watanabe, K., Sakaguchi, I., 2017. Hydrogen diffusion in the apatite-water system: fluorapatite parallel to the *c*-axis. Geochem. J. 51, 115–122. https://doi.org/10.2343/geochemj.2.0460.

Hughes, J.M., Rakovan, J.F., 2015. Structurally robust, chemically diverse: apatite and apatite supergroup minerals. Elements 11, 165–170. https://doi.org/10.2113/gselements.11.3.165.

Hughes, J.M., Cameron, M., Crowley, K.D., 1989. Structural variations in natural F, OH, and Cl apatites. Am. Mineral. 74, 870–876.

Li, W., Chakraborty, S., Nagashima, K., Costa, F., 2020. Multicomponent diffusion of F, Cl and OH in apatite with application to magma ascent rates. Earth Planet. Sci. Lett. 550, 116545. https://doi.org/10.1016/j.epsl.2020.116545.

McCubbin, F.M., Nekvasil, H., 2008. Maskelynite-hosted apatite in the Chassigny meteorite: Insights into late-stage magmatic volatile evolution in martian magmas. Am. Mineral. 93, 676–684. https://doi.org/10.2138/am.2008.2558.

McCubbin, F.M., Steele, A., Hauri, E.H., Nekvasil, H., Yamashita, S., Hemley, R.J., 2010. Nominally hydrous magmatism on the Moon. Proc. Natl. Acad. Sci. 107, 11223–11228. https://doi.org/10.1073/pnas.1006677107.

McCubbin, F.M., Vander Kaaden, K.E., Tartèse, R., Klima, R.L., Liu, Y., Mortimer, J., Barnes, J.J., Shearer, C.K., Treiman, A.H., Lawrence, D.J., Elardo, S.M., Hurley, D. M., Boyce, J.W., Anand, M., 2015. Magmatic volatiles (H, C, N, F, S, Cl) in the lunar mantle, crust, and regolith: Abundances, distributions, processes, and reservoirs. Am. Mineral. 100, 1668–1707. https://doi.org/10.2138/am-2015-4934CCBYNCND.

Momma, K., Izumi, F., 2008. VESTA: a three-dimensional visualization system for electronic and structural analysis. J. Appl. Crystallogr. 41, 653–658.

Norby, T., Larring, Y., 1997. Concentration and transport of protons in oxides. Curr. Opin. Solid State Mater. Sci. 2, 593–599. https://doi.org/10.1016/S1359-0286(97)80051-4.

Piccoli, P., Candela, P., 1994. Apatite in felsic rocks; a model for the estimation of initial halogen concentrations in the Bishop Tuff (Long Valley) and Tuolumne Intrusive Suite (Sierra Nevada Batholith) magmas. Am. J. Sci. 294, 92–135.

Sakaguchi, I., Yurimoto, H., Sueno, S., 1992. Impurities dislocation diffusion in single-crystal MgO. Mater. Sci. Eng. B 13, L1–L4. https://doi.org/10.1016/0921-5107(92)90175-9.

Steele, I.M., Smith, J.V., 1982. Petrography and mineralogy of two basalts and olivine-pyroxene-spinel fragments in achondrite EETA79001. J. Geophys. Res. Solid Earth 87. https://doi.org/10.1029/JB087iS01p0A375.

Suzuoki, T., Epstein, S., 1976. Hydrogen isotope fractionation between OH-bearing minerals and water. Geochim. Cosmochim. Acta 40, 1229–1240. https://doi.org/10.1016/0016-7037(76)90158-7.

Tetens, O., 1930. Uber einige meteorologische Begriffe. Z. Geophys. 6, 297–309.

Yaqian, Q., Jibao, G., 1993. Study of hydrogen isotope equilibrium and kinetic fractionation in the ilvaite-water system. Geochim. Cosmochim. Acta 57, 3073–3082. https://doi.org/10.1016/0016-7037(93)90294-7.

Yokoyama, T., Nagashima, K., Nakai, I., Young, E.D., Abe, Y., Aléon, J., Alexander, C.M. O., Amari, S., Amelin, Y., Bajo, K., Bizzarro, M., Bouvier, A., Carlson, R.W., Chaussidon, M., Choi, B.-G., Dauphas, N., Davis, A.M., Di Rocco, T., Fujiya, W., Fukai, R., Gautam, I., Haba, M.K., Hibiya, Y., Hidaka, H., Homma, H., Hoppe, P., Huss, G.R., Ichida, K., Iizuka, T., Ireland, T.R., Ishikawa, A., Ito, M., Itoh, S., Kawasaki, N., Kita, N.T., Kitajima, K., Kleine, T., Komatani, S., Krot, A.N., Liu, M.-C., Masuda, Y., McKeegan, K.D., Morita, M., Motomura, K., Moynier, F., Nguyen, A., Nittler, L., Onose, M., Pack, A., Park, C., Piani, L., Qin, L., Russell, S.S., Sakamoto, N., Schönbächler, M., Tafla, L., Tang, H., Terada, K., Terada, Y., Usui, T., Wada, S., Wadhwa, M., Walker, R.J., Yamashita, K., Yin, Q.-Z., Yoneda, S., Yui, H., Zhang, A.-C., Connolly, H.C., Lauretta, D.S., Nakamura, T., Naraoka, H., Noguchi, T., Okazaki, R., Sakamoto, K., Yabuta, H., Abe, M., Arakawa, M., Fujii, A., Hayakawa, M., Hirata, Naoyuki, Hirata, Naru, Honda, R., Honda, C., Hosoda, S., Iijima, Y., Ikeda, H., Ishiguro, M., Ishihara, Y., Iwata, T., Kawahara, K., Kikuchi, S., Kitazato, K., Matsumoto, K., Matsuoka, M., Michikami, T., Mimasu, Y., Miura, A., Morota, T., Nakazawa, S., Namiki, N., Noda, H., Noguchi, R., Ogawa, N., Ogawa, K., Okada, T., Okamoto, C., Ono, G., Ozaki, M., Saiki, T., Sakatani, N., Sawada, H., Senshu, H., Shimaki, Y., Shirai, K., Sugita, S., Takei, Y., Takeuchi, H., Tanaka, S., Tatsumi, E., Terui, F., Tsuda, Y., Tsukizaki, R., Wada, K., Watanabe, S., Yamada, M., Yamada, T., Yamamoto, Y., Yano, H., Yokota, Y., Yoshihara, K., Yoshikawa, M., Yoshikawa, K., Furuya, S., Hatakeda, K., Hayashi, T., Hitomi, Y., Kumagai, K., Miyazaki, A., Nakato, A., Nishimura, M., Soejima, H., Suzuki, A., Yada, T., Yamamoto, D., Yogata, K., Yoshitake, M., Tachibana, S., Yurimoto, H., 2022. Samples returned from the asteroid Ryugu are similar to Ivuna-type carbonaceous meteorites. Science 379, eabn7850. https://doi.org/10.1126/science.abn7850.

Yoshimoto, C., Itoh, S., Sakaguchi, I., 2024. Hydrogen diffusion in apatite parallel to the c-axis under vapor flow. Geochem. J. 58, 1–8. https://doi.org/10.2343/geochemj.GJ24001.

Young, E., Myers, A., Munson, E.L., Conklin, N.M., 1969. Geological survey research 1969. In: US Geological Survey Professional Paper. US Government Printing Office, p. 84.

Yurimoto, H., Morioka, M., Nagasawa, H., 1989. Diffusion in single crystals of melilite: I. Oxygen. Geochim. Cosmochim. Acta 53, 2387–2394. https://doi.org/10.1016/0016-7037(89)90360-8.

Zhang, X.Y., Watson, E.B., Cherniak, D.J., 2007. Oxygen self-diffusion “fast-paths” in titanite single crystals and a general method for deconvolving self-diffusion profiles with “tails”. Geochim. Cosmochim. Acta 71, 1563–1573.